Inorganic Chemistry

Article

pubs.acs.org/IC

Synthesis of Panchromatic Ru(II) Thienyl-Dipyrrin Complexes and Evaluation of Their Light-Harvesting Capacity

Guocan Li,[†] Lipika Ray,[†] Elliot N. Glass,[†] Kirill Kovnir,[†,⊥] Andrey Khoroshutin,[§] Serge I. Gorelsky,*[,‡] and Michael Shatruk*[,†]

[†]Department of Chemistry and Biochemistry, Florida State University, Tallahassee, Florida 32306, United States

[‡]Centre for Catalysis Research and Innovation, Department of Chemistry, University of Ottawa, Ottawa, Ontario K1N 6N5, Canada

[§]Petroleum Chemistry Division, Department of Chemistry, M. V. Lomonosov Moscow State University, Moscow, 119991, Russia

Supporting Information

ABSTRACT: Ru(II) complexes with 5-(3-thienyl)-4,6-dipyrrin (3-TDP), containing 2,2′-bipyridine (bpy) or 4,4′-bis-(methoxycarbonyl)-2,2′-bipyridine (dcmb) as coligands, have been prepared and extensively characterized. Crystal structure determination of $[Ru(bpy)_2(3\text{-}TDP)]PF_6$ (**1a**) and $[Ru(bpy)_2(3\text{-}TDP)_2]$ (**2**) reveals that the 3-thienyl substituent is rotated with respect to the plane of the dipyrrinato moiety. These complexes, as well as $[Ru(dcmb)_2(3\text{-}TDP)]PF_6$ (**1b**), act as panchromatic light absorbers in the visible range, with two strong absorption bands observable in each case. A comparison to known Ru(II) complexes and quantum-chemical calculations at the density functional theory (DFT) level indicate that the lower-energy band is due to metal-to-ligand charge transfer (MLCT) excitation, although the frontier occupied metal-based molecular orbitals (MOs) contain significant contributions from the 3-TDP moiety. The higher energy band is assigned to the $\pi-\pi^*$ transition of the 3-TDP ligand. Each complex exhibits an easily accessible one-electron oxidation. According to DFT calculations and spectroelectrochemical experiments, the first oxidation takes place at the Ru^{II} center in **1a**, but is shifted to the 3-TDP ligand in **1b**. An analysis of MO energy diagrams suggests that complex **1b** has potential to be used for light harvesting in the dye-sensitized (Grätzel) solar cell.

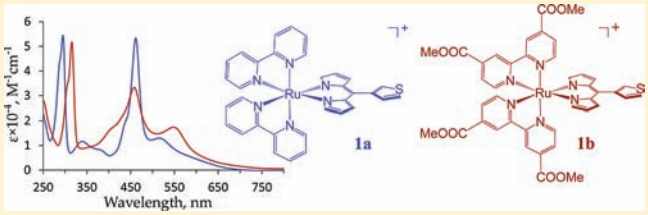

INTRODUCTION

In recent years, the growing awareness of fossil fuel depletion has boosted efforts in exploring alternative energy sources. Among these, dye-sensitized solar cells (DSSCs) originally developed by Grätzel[1] have attracted considerable interest owing to their low fabrication cost and high efficiency.[2] In a DSSC device (Scheme 1), photoexcitation of a dye-sensitizer results in electron injection into the conduction band of a nanocrystalline wide-band gap semiconductor (typically TiO_2). The injected electrons are transferred to the cathode and then via an external load to the anode, where they are transported by means of a reversible redox couple (typically I_3^-/I^-) to regenerate the dye and complete the electrical circuit. One of the most significant indicators of the device performance is the overall energy conversion efficiency, defined as the ratio of output electrical energy to the input sunlight energy. Under AM 1.5 simulated solar light irradiation, the overall energy conversion efficiency as high as ∼11% has been achieved.[3] The efficiency is dependent, to a considerable degree, on the absorptivity of the dye, making it the key component of the device. The benchmark typically used to evaluate the performance of new dyes is $Ru(dcbpy)_2(NCS)_2$ (dcbpy = 4,4′-dicarboxylato-2,2′-bipyridine), commonly referred to as N3.[4]

Ruthenium polypyridyl complexes have been extensively used as sensitizers in DSSCs owing to their strong absorption in the visible range and relatively long-lived excited states.[5] The strong absorptivity of these complexes is due to a metal-to-ligand

Scheme 1. Operation Diagram of a Dye-Sensitized Solar Cell[a]

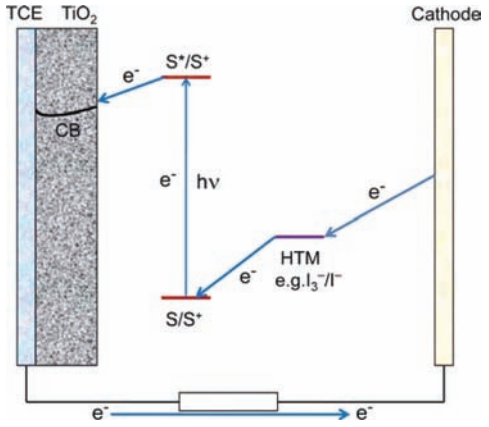

[a]S = sensitizer; TCE = transparent conducting electrode; HTM = hole transporting material.

Received: September 1, 2011
Published: January 17, 2012

 © 2012 American Chemical Society dx.doi.org/10.1021/ic2019204 | Inorg. Chem. 2012, 51, 1614−1624

Scheme 2. Molecular Structures of Ru(II) Complexes Reported in This Work

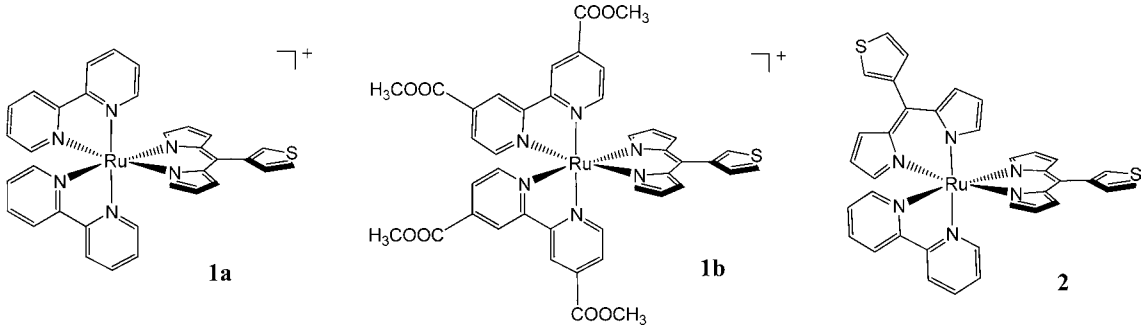

charge transfer (MLCT) transition, in which an electron is transferred from the t_{2g} orbital of the Ru^{II} center to the π^* orbital of a polypyridyl ligand. This transition leads to efficient charge separation, which consequently facilitates the charge injection process while suppressing unwanted charge recombination. To improve light harvesting and hence the DSSC efficiency, the absorbance of the MLCT band should be maximized. This requires increasing the extinction coefficient of the MLCT band and shifting its maximum to longer wavelengths. The latter can be realized by using ancillary σ- and/or π-donor ligands, which raise the energy of Ru^{II} t_{2g} orbitals and reduce the energy gap between the highest occupied and lowest unoccupied molecular orbitals (HOMO and LUMO). Thus, thiocyanate (SCN^-) has been successfully used as an ancillary ligand in many ruthenium sensitizers.[3,4,6−9] Such Ru(II) polypyridyl complexes, however, suffer from the lability of the thiocyanate ligand, which decreases the dye's stability.[10,11] Attempts to use alternative ligands have led to limited success thus far. Nevertheless, the recent use of chelating 2-phenylpyridine in place of thiocyanates resulted in dyes with efficiencies comparable to that of N3.[10,12,13] Other efforts have been directed at increasing the absorptivity of the MLCT band. In particular, it has been shown that the molar extinction coefficient (ε) can be increased by introduction of thiophene moieties on the periphery of polypyridyl ligands.[14,15] Until now, however, very few Ru(II) complexes incorporating thienyl substituents exhibit ε_{MLCT} higher than 2.0×10^4 M^{-1} cm^{-1}.[16,17]

Dipyrromethenes, or dipyrrins, exhibit strong absorption in the visible range and have been used extensively in combination with Lewis acidic boron species (known as BODIPY) for laser and biological applications,[18] and also as solar cell sensitizers.[19−21] Dipyrrins act as monoanionic chelating ligands[22] and in this way are similar to 2-phenylpyridines. Surprisingly, the first Ru(II) polypyridyl complexes of dipyrrinato ligand have been reported only recently.[23,24] $[Ru(bpy)_2(4\text{-MCDP})](PF_6)$ (bpy = 2,2′-bipyridine, 4-MCDP = 4-methoxycarbonylphenyl-dipyrrinato) described by Telfer, Waterland, et al.[23] exhibits absorption bands in the visible range owing both to the Ru to bpy MLCT transition and to the dipyrrin $\pi-\pi^*$ transition. The complex thus acts as strong panchromatic light absorber, although its usefulness for light-harvesting applications is yet to be elucidated.[25]

The fascinating photophysical characteristics of dipyrrins incited us to explore their Ru(II) complexes as potential DSSC sensitizers. Furthermore, we decided to use for this purpose 5-(3- thienyl)-4,6-dipyrrin (3-TDP), keeping in mind that the presence of electron-donating substituents usually improves the charge separation.[26] This ligand, therefore, potentially offers four advantages to the design of a panchromatic dye: (1) the σ/π-donating nature of the dipyrrinato ligand will cause a shift of the MLCT band to the longer wavelengths, making it comparable to the MLCT band of thiocyanato-containing complexes; (2) the chelating nature of the ligand should impart higher stability to the resulting complex as compared to thiocyanato-containing dyes; (3) in addition to the MLCT band, another high-intensity band should appear in the absorption spectrum of the complex because of the dipyrrinato ligand; (4) the introduction of the thienyl substituent will provide for improved charge separation in the MLCT excited state, decreasing the probability of charge recombination.

Herein, we report the preparation and extensive characterization of Ru(II) complexes (Scheme 2) incorporating the 3-TDP ligand: $[Ru(bpy)_2(3\text{-TDP})]PF_6$ (**1a**) and $[Ru(bpy)(3\text{-TDP})_2]$ (**2**), and a carboxylated analogue, $[Ru(dcmb)_2(3\text{-TDP})]PF_6$ (**1b**, dcmb = 4,4′-bis(methoxycarbonyl)-2,2′-bipyridine). An analysis of electrochemical and optical properties aided by quantum-chemical calculations demonstrates that the reported complexes offer a promising direction for the development of new DSSC sensitizers.

EXPERIMENTAL SECTION

Spectroscopic Measurements. ^1H nuclear magnetic resonance (NMR) spectra were measured on Bruker 400 and 600 MHz spectrometers. Chemical shifts were referenced to the signals of residual protons in deuterated solvents (7.26 ppm in $CDCl_3$ and 2.50 ppm in DMSO-d_6).[27] Electrospray ionization (ESI) mass spectra were acquired on a Beckman Coulter System Gold HPLC BioEssential with Binary Gradient 125S pump and a UV/vis 166 analytical detector. Electronic absorption (UV−vis) spectra were collected in the 200−1000 nm range on a Perkin-Elmer Lambda 950 UV/vis/NIR spectrophotometer.

Electrochemistry. Cyclic voltammograms (CV) were recorded on a CH Instruments 600D electrochemical analyzer at the sweep rate of 0.100 $V \cdot s^{-1}$, with 0.100 M $(TBA)PF_6$ electrolyte solution (TBA = tetrabutylammonium), Pt working electrode, and Ag^+(0.01 M $AgNO_3$)/Ag reference electrode. All the potentials initially were referenced to the standard Fc^+/Fc couple (Fc = ferrocene). Fc was added as an internal standard upon completion of each CV experiment. The redox potentials reported in this work have been converted to the normal hydrogen electrode (NHE), assuming that the Fc^+/Fc couple has a redox potential of +0.630 V vs NHE in acetonitrile.[28] Spectroelectrochemical measurements were performed on a Shimadzu UV-2450 spectrophotometer, using a commercial thin-layer cell with a Pt mesh electrode (BASi). The spectra were collected in the 300−750 nm range for various applied potentials after reaching redox equilibrium at each specific potential value.

Syntheses. All reactions were performed in an inert (N_2) atmosphere using standard Schlenk techniques, unless noted otherwise. All reagents were purchased from Aldrich, except for $RuCl_3 \cdot 3H_2O$ (Pressure Chemical Company), pyrrole (Alfa Aesar), and

dx.doi.org/10.1021/ic2019204 | Inorg. Chem. 2012, 51, 1614−1624

α-phellandrene (TCI), and they were used as received, except for pyrrole which was distilled prior to use. 5-(3-thienyl)-4,6-dipyrromethane,[29] 4,4′-bis(methoxycarbonyl)-2,2′-bipyridine (dcmb),[30] [(*p*-cymene)$RuCl_2]_2$,[31] and $Ru(dmso)_4Cl_2$[32] were prepared according to published procedures. Anhydrous commercial solvents were additionally purified by passing through a double-stage drying/purification system (Glass Contour Inc.). Elemental analyses were performed by Atlantic Microlab, Inc. (Atlanta, GA).

5-(3-Thienyl)-4,6-dipyrrin (3-TDP). A 700 mg portion (2.85 mmol) of *p*-chloranil (tetrachloro-1,4-benzoquinone) was dissolved in 20 mL of anhydrous tetrahydrofuran (THF) and transferred dropwise over a period of 1 h to a solution of 5-(3-thienyl)-4,6-dipyrromethane (650 mg, 2.85 mmol) in 10 mL of anhydrous THF under vigorous stirring. The solution gradually turned from light-yellow to yellow-brown. The stirring was continued for another 17 h at room temperature, after which time the solvent was removed under reduced pressure. The residue was charged on a silica gel chromatography column. After washing off impurities with a CH_2Cl_2:hexanes:ethyl acetate = 10:10:1 mixture, the major yellow-brown fraction was collected by elution with a CH_2Cl_2:hexanes:ethyl acetate = 1:1:1 mixture. The solvent was evaporated to dryness to afford 512 mg of a brown solid. Yield = 80%. *^{1}H NMR* ($CDCl_3$, 600 MHz), *δ*, ppm: 7.65 (s, 2H), 7.52 (dd, 1H, *J* = 3.0, 1.1 Hz), 7.39–7.41 (m, 1H), 7.31 (dd, 1H, *J* = 5.0, 1.2 Hz), 6.80 (dd, 2H, *J* = 4.2, 1.4 Hz), 6.41 (dd, 2H, *J* = 4.1, 1.4 Hz). *^{13}C NMR* ($CDCl_3$, 151 MHz), *δ*, ppm: 143.7, 140.8, 137.9, 130.8, 128.7, 128.0, 126.2, 117.7, 29.9. *HR-ESI-MS*: *m*/*z* = 227.06391 (calcd. for $[3\text{-TDP+H}]^+$: 227.06429).

(*p*-Cymene)Ru(3-TDP)Cl. A 340 mg portion (0.56 mmol) of [(*p*-cymene)$RuCl_2]_2$ and 249 mg (1.10 mmol) of 3-TDP were added to a 100 mL Schlenk flask, followed by 1 mL of Et_3N and 30 mL of anhydrous CH_3CN. The mixture was heated at reflux for 14 h. After cooling down to room temperature, the solvent was removed under reduced pressure, and the residue was charged on a silica gel column (2.5 cm × 20 cm). The separation was achieved using CH_2Cl_2:MeOH (50:1 v/v) as eluent. A bright-red fraction was collected and evaporated to dryness to yield 240 mg of a red solid. Yield = 44%. *^{1}H NMR* ($CDCl_3$, 600 MHz), *δ*, ppm: 8.00 (s, 2H), 7.39 (dd, 1H, *J* = 3.0, 1.2 Hz), 7.33–7.35 (m, 1H), 7.21 (dd, 1H, *J* = 4.9, 0.8 Hz), 6.78 (dd, 2H, *J* = 4.3, 0.8 Hz), 6.48 (dd, 2H, *J* = 4.4, 1.1 Hz), 5.28 (d, 4H, *J* = 1.5 Hz), 2.42 (sep, 1H), 2.22 (s, 3H), 1.07 (d, 6H, *J* = 6.9 Hz). *^{13}C NMR* ($CDCl_3$, 151 MHz), *δ*, ppm: 154.9, 141.5, 138.3, 135.2, 131.0, 130.9, 126.7, 124.3, 118.4, 102.3, 100.4, 85.0, 84.8, 30.7, 22.2, 18.7. *HR-ESI-MS*: *m*/*z* = 461.06314 (calcd. for [(*p*-cymene)Ru(3-TDP)]$^+$: 461.06254).

[Ru(bpy)$_2$(3-TDP)](PF$_6$) (1a). *Method A.* A mixture of (*p*-cymene)-Ru(3-TDP)Cl (30 mg, 0.061 mmol), bpy (20 mg, 0.128 mmol), and $AgNO_3$ (11 mg, 0.065 mmol) was added to a 100 mL Schlenk flask, followed by 20 mL of anhydrous EtOH. The mixture was heated at reflux in the dark for 20 h. After cooling down to room temperature, AgCl was removed by filtering through Celite, and the filtrate was concentrated to ∼5 mL. A solution of NH_4PF_6 (20 mg, 0.123 mmol) in 2 mL of EtOH was added, and the mixture was stirred vigorously for 30 min to complete the anion exchange. The solution was filtered through a medium porosity frit, and the product was washed with diethyl ether (3 × 10 mL) and dried in vacuum to afford 30 mg of black crystalline solid. Yield = 70%. Single crystals suitable for X-ray diffraction were obtained by slow evaporation of a $CHCl_3$ solution of the complex. *^{1}H NMR* ($CDCl_3$, 600 MHz), *δ*, ppm: 8.34–8.35 (m, 4H), 7.86–7.90 (m, 6H), 7.70 (dd, 2H, *J* = 5.6, 0.6 Hz), 7.42 (dd, 1H, *J* = 3.0, 1.2 Hz), 7.36–7.38 (m, 1H), 7.28–7.31 (m, 4H), 7.24 (dd, 1H, *J* = 4.9, 1.2 Hz), 6.83 (dd, 2H, *J* = 4.4, 1.2 Hz), 6.36–6.37 (m, 2H), 6.30 (dd, 2H, *J* = 4.4, 1.4 Hz). *^{13}C NMR* ($CDCl_3$, 151 MHz), *δ*, ppm: 157.9, 157.3, 151.8, 150.8, 149.0, 142.0, 136.1, 135.7, 135.5, 131.4, 131.0, 126.8, 126.6, 126.2, 124.2, 123.4, 123.3, 118.2. *HR-ESI-MS*: *m*/*z* = 639.09005 (calcd. for $[Ru(bpy)_2(3\text{-TDP})]^+$: 639.09049). *UV–vis* ($CH_3CN$), λ_{max}, nm (*ε*, M^{-1} cm^{-1}): 295 (5.5×10^4), 339 (1.2×10^4), 375 (8.4×10^3), 462 (5.3×10^4), 516 (1.3×10^4). *Elem. analysis*: calcd. (found) for $RuSPF_6N_6C_{33}H_{26}O_{0.5}$ (**1a**·0.5H_2O), %: C, 50.00 (50.07); H, 3.31 (3.09); N, 10.60 (10.50).

Method B. A 190 mg portion (0.84 mmol) of 3-TDP and 407 mg (0.84 mmol) of $Ru(bpy)_2Cl_2$ were added to a 100 mL Schlenk flask, followed by 0.60 mL of Et_3N and 20 mL of anhydrous EtOH. The reaction mixture was heated at reflux in the dark overnight. After cooling down to room temperature, the mixture was filtered through a medium porosity frit, and the filtrate was concentrated to ∼5 mL under reduced pressure. A solution of 452 mg (2.77 mmol) of NH_4PF_6 in 3 mL of EtOH was added, and the mixture was left undisturbed in a freezer at −23 °C overnight. The precipitate that formed was collected by filtering through a medium porosity frit and washed successively with diethyl ether (3 × 20 mL) and hexanes (3 × 20 mL). Then, the solid was charged on a neutral alumina column (3 cm × 20 cm). CH_2Cl_2:ethyl acetate (1:1 v/v) was used to elute the first yellow fraction, and then the eluent was changed to ethyl acetate:MeOH (10:1 v/v) to collect a red-brown product fraction, which was evaporated to dryness to afford 128 mg of black solid. Yield = 28%.

[Ru(dcmb)$_2$(3-TDP)]PF$_6$ (1b). (*p*-cymene)Ru(3-TDP)Cl (90 mg, 0.18 mmol), dcmb (124 mg, 0.46 mmol), and $AgNO_3$ (40 mg, 0.24 mmol) were added to a 100 mL Schlenk flask, followed by 30 mL of anhydrous MeOH. The mixture was heated at reflux in the dark for 17 h, after which time NMR indicated all the starting material (*p*-cymene)Ru(3-TDP)Cl had been consumed. After cooling down to room temperature, the mixture was concentrated to ∼5 mL and filtered through a fine porosity frit to remove AgCl and excess dcmb. A 2 mL MeOH solution of NH_4PF_6 (80 mg, 0.49 mmol) was added to the filtrate, and the mixture was stirred vigorously for 30 min to complete the anion exchange. The product was collected by filtration through a medium porosity frit, washed with diethyl ether (3 × 10 mL), and dried in vacuum to afford 140 mg of black powder. Yield = 76%. *^{1}H NMR* ($CDCl_3$, 600 MHz), *δ*, ppm: 8.88 (d, 4H, *J* = 13.0 Hz), 7.98 (dd, 4H, *J* = 19.6, 5.9 Hz), 7.90 (d, 4H, *J* = 5.9 Hz), 7.41 (d, 1H, *J* = 2.6 Hz), 7.37–7.39 (m, 1H), 7.21 (d, 1H, *J* = 4.9 Hz), 6.83 (d, 2H, *J* = 4.4 Hz), 6.28 (d, 2H, *J* = 4.4 Hz), 6.25 (s, 2H), 4.05 (s, 6H), 4.01 (s, 6H). *^{13}C NMR* ($CDCl_3$, 151 MHz), *δ*, ppm: 164.1, 158.3, 157.5, 152.6, 152.4, 149.1, 142.8, 137.7, 137.1, 135.9, 132.4, 131.1, 127.2, 126.8, 126.0, 124.7, 123.2, 122.9, 118.9, 53.6. *HR-ESI-MS*: *m*/*z* = 871.11151 (calcd. for $[Ru(dcmb)_2(3\text{-TDP})]^+$: 871.11241). *UV–vis* ($CH_3CN$), λ_{max}, nm (*ε*, M^{-1} cm^{-1}): 316 (5.2×10^4), 458 (3.3×10^4), 548 (1.7×10^4). *Elem. analysis*: calcd. (found) for $RuSPF_6O_{10}N_6C_{41}H_{37}$ (**1b**·2H_2O), %: C, 46.82 (46.77); H, 3.55 (3.35); N, 7.99 (8.09); S, 3.05 (3.04).

Ru(dmso)$_2$(3-TDP)$_2$. A 78 mg portion (0.16 mmol) of $Ru(dmso)_4Cl_2$ and 91 mg (0.40 mmol) of 3-TDP were added to a 100 mL Schlenk flask, followed by 0.28 mL of Et_3N. The mixture was heated at reflux for 24 h. After cooling down to room temperature, an insoluble black solid was removed by passing the mixture through Celite. The solvent was removed under reduced pressure, and the obtained solid was redissolved in 20 mL of acetone. The solution was passed through Celite to remove unreacted $Ru(dmso)_4Cl_2$. The filtrate was evaporated to dryness, and the residue was charged on a silica gel column (2.5 cm × 18 cm). Using CH_2Cl_2:ethyl acetate (2:1 v/v) as eluent, an orange-red product fraction was collected and evaporated to dryness, affording 52 mg of orange solid. Yield = 46%. *^{1}H NMR* ($CDCl_3$, 600 MHz), *δ*, ppm: 8.8 (s, 2H), 7.33–7.35 (m, 4H), 7.18 (dd, 2H, *J* = 4.6, 1.5 Hz), 6.85 (dd, 2H, *J* = 4.4, 1.3 Hz), 6.67 (d, 2H, *J* = 3 Hz), 6.54 (dd, 2H, *J* = 4.4, 1.6 Hz), 6.45 (s, 2H), 6.21 (dd, 2H, *J* = 4.3, 1.5 Hz), 2.77 (s, 6H), 2.51 (s, 6H). *^{13}C NMR* ($CDCl_3$, 151 MHz), *δ*, ppm: 155.6, 152.2, 141.6, 139.3, 136.7, 135.8, 132.4, 132.1, 126.4, 124.1, 118.4, 118.3, 45.8, 45.5. *HR-ESI-MS*: *m*/*z* = 708.06951 (calcd. for $[Ru(dmso)_2(3\text{-TDP})_2]^+$: 708.02951).

Ru(bpy)(3-TDP)$_2$ (2). Anhydrous EtOH (10 mL) was added to a 50 mL Schlenk flask containing 50 mg (0.071 mmol) of $Ru(dmso)_2$-$(3\text{-TDP})_2$ and 11 mg (0.071 mmol) of bpy. The mixture was heated at reflux in the dark for 48 h. After cooling down to room temperature, the obtained dark-green mixture was filtered through a medium porosity frit, and the filter cake was washed thoroughly with EtOH and dried, affording 27 mg of dark-green solid. Yield = 54%. Single crystals suitable for X-ray diffraction were obtained by slow evaporation of a $CHCl_3$ solution of the complex. *^{1}H NMR* ($CDCl_3$, 400 MHz), *δ*, ppm: 8.18 (d, 2H, *J* = 5.3 Hz), 8.02 (d, 2H, *J* = 8.1 Hz), 7.59 (td, 2H, *J* = 7.8, 1.5 Hz), 7.41 (dd, 2H, *J* = 3.0, 1.2 Hz), 7.31 (dd, 2H, *J* = 4.9, 3.0 Hz), 7.27 (d, 2H, *J* = 1.3 Hz), 7.12 (t, 2H, *J* = 6.0 Hz), 6.79 (d, 2H, *J* = 3.9 Hz), 6.69–6.63 (m, 4H), 6.37–6.31 (m, 4H), 6.18 (dd, 2H, *J* = 4.2,

dx.doi.org/10.1021/ic2019204 | *Inorg. Chem.* 2012, 51, 1614–1624

1.5 Hz). ^{13}C *NMR* ($CDCl_3$, 151 MHz), δ, ppm: 153.8, 148.2, 140.9, 140.1, 133.8, 131.1, 126.6, 125.4, 123.7, 120.1, 114.9. *HR-ESI-MS*: m/z = 708.07271 (calcd. for $[Ru(bpy)(3\text{-}TDP)_2]^+$: 708.07038). *UV−vis* ($CH_3CN$), λ_{max}, nm (ε, M^{-1} cm^{-1}): 298 (2.4×10^4), 318 (1.0×10^4), 450 (5.9×10^4), 636 (6.2×10^3). *Elem. analysis*: calcd. (found) for $RuS_2N_6C_{36}H_{27}O_{0.5}$ (**2**·0.5H_2O), %: C, 60.32 (60.25); H, 3.80 (3.79); N, 11.72 (11.60); S, 8.95 (8.97).

X-ray Crystallography. In a typical experiment, a single crystal was suspended in Paratone-N oil (Hampton Research) and mounted on a cryoloop, which was placed in an N_2 cold stream and cooled down at 5 K/min to the desired temperature. The data sets were recorded as ω-scans at 0.3° stepwidth and integrated with the Bruker SAINT software package.[33] In all the experiments, a multiscan adsorption correction was applied based on fitting a function to the empirical transmission surface as sampled by multiple equivalent measurements (SADABS).[34] Determination of the space group, solution and refinement of the crystal structures were carried out using the SHELX suite of programs.[35] The final refinement was performed with anisotropic atomic displacement parameters for all non-hydrogen atoms. The H atoms were placed in calculated positions. A summary of pertinent information relating to unit cell parameters, data collection, and refinements is provided in Table 1.

Table 1. Data Collection and Structure Refinement Parameters for 1a and 2

formula	$RuCl_6SPF_6N_{61}C_{35}H_{27}$ (**1a**·2$CHCl_3$)	$RuS_2N_6C_{36}H_{26}$ (**2**)
CCDC no.	809972	809973
space group	$P\bar{1}$	*Pbcn*
unit cell parameters, Å and deg	a = 11.126(1) b = 12.655(1) c = 15.996(2) α = 100.964(1) β = 101.365(1) γ = 104.782(1)	a = 12.9812(8) b = 10.7751(7) c = 21.541(1)
V, Å^3	2065.2(4)	3013.0(3)
Z	2	4
ρ_{calc}, g cm^{-3}	1.644	1.560
μ, mm^{-1}	0.920	0.697
Temperature	153 K	153 K
λ, Å	Mo$K\alpha$, 0.71073	
$2\theta_{max}$, deg	25.0	26.0
reflections collected	19502	18506
R_{int}	0.019	0.019
unique reflections	7244	2964
parameters refined	612	220
restraints used	48	5
R_1, wR_2 [$F_o > 4\sigma(F_o)$]	0.042, 0.108	0.022, 0.059
goodness-of-fit	1.071	1.055
diff. peak and hole, e/Å^3	0.83 and −0.48	0.44 and −0.36

Theoretical Calculations. Density functional theory (DFT) calculations were performed with the Gaussian 09 package,[36] using the B3LYP hybrid functional[37,38] and the DZVP basis set[39] for Ru and the TZVP basis set[40] for the other elements. Open- and closed-shell species were calculated using spin-unrestricted and spin-restricted molecular orbital (MO) models, respectively. Starting geometries for complexes **1a** and **2** were taken from the refined crystal structure parameters. Calculations for complex **1b** were performed by adding carboxylic acid functionalities (−COOH) to bpy ligands of complex **1a**. All geometries were optimized in the ground state, without symmetry restraints, using the conducting polarized continuum medium (PCM, acetonitrile) model to include solvent polarization effects. Time-dependent (TD) DFT calculations in solution (also using the PCM model) were carried out on the optimized geometries. The UV−vis spectra were calculated with the SWizard program, revision 4.6,[41,42] using the pseudo-Voigt model (50% Gaussian/50% Lorentzian). The half-bandwidths, $\Delta_{1/2}$, were taken to be equal to 3000 cm^{-1}. Atomic/fragment contributions to the MOs were calculated using the AOMix software.[42,43]

RESULTS AND DISCUSSION

Syntheses. 5-(3-Thienyl)-4,6-dipyrromethane was prepared from 3-thienylcarboxaldehyde and pyrrole according to the published procedure.[29] The oxidation of dipyrromethane to dipyrrin also followed the reported procedure,[44] but instead of DDQ (2,3-dichloro-5,6-dicyanobenzoquinone) we used a milder oxidizing agent, *p*-chloranil (tetrachloro-1,4-benzoquinone), which afforded a much higher yield. A reaction between dipyrrin and $Ru(bpy)_2Cl_2$ in the presence of deprotonating reagent (Et_3N) in refluxing ethanol results in the replacement of chloride ions and isolation of **1a** as microcrystalline solid after addition of excess NH_4PF_6 (yield = 28% based on $Ru(bpy)_2Cl_2$). A similar procedure using $Ru(dcmb)_2Cl_2$ failed to produce **1b**. Hence, an alternative method was used, in which $[(p\text{-cymene})RuCl_2]_2$ is converted to (*p*-cymene)Ru(3-TDP)Cl, followed by one-pot abstraction of chloride with $AgNO_3$ and introduction of dcmb to afford **1b** in an overall yield of 33% based on $[(p\text{-cymene})RuCl_2]_2$. **1a** was also successfully synthesized following this procedure and using bpy instead of dcmb (yield = 31% based on $[(p\text{-cymene})RuCl_2]_2$). The advantage of the latter method is easier purification of the final product. Complex **2** was synthesized in two steps. A reaction between $Ru(dmso)_4Cl_2$ and 3-TDP in a 1:2 ratio produced a neutral complex $Ru(dmso)_2(3\text{-}TDP)_2$, which was then reacted with bpy in a 1:1 ratio to afford **2** as dark-green solid, with the overall yield of 25% based on $Ru(dmso)_4Cl_2$.

NMR Spectroscopy. The identities of the ligands and complexes were verified by NMR spectroscopy. To allow conclusive assignment of NMR signals, 2-D COSY spectra were also collected, in addition to conventional 1-D NMR spectra (Supporting Information, Figure S1). The aromatic region of the spectra contains signals that can be assigned to bipyridine, dipyrrinato, and thienyl moieties. Upon coordination of dipyrrinato ligand to the Ru^{II} center, the most dramatic changes are observed for the protons on the dipyrrinato moiety, which are shifted upfield, while the thienyl protons are much less affected, being more remote from the Ru^{II} center. The largest change is observed for the dipyrrinato α-protons (Figure 1), whose signal is shifted upfield by ∼1.3 ppm. This shift can be explained by shielding arising from the proximity of these protons to the π-system of bpy ligands (Supporting Information, Figure S3).

In all complexes, the dipyrrinato protons appear in a distinct region, upfield from the other aromatic protons. In comparison to **1a**, in which the signals from thienyl and bpy protons partially overlap, in **1b** they are clearly separated. This separation is due to the downfield shift of bpy protons caused by the electron-withdrawing effect of the ester groups. The largest downfield shift is observed for the protons next to the ester groups, while the shift of the other protons is relatively small (Figure 1).

The positions of dipyrrinato proton signals of bisdipyrrinato complex **2** are similar to those observed in monodipyrrinato complex **1a**. Nevertheless, the presence of the second 3-TDP ligand causes the splitting of the α-proton doublet into two singlets, while one of the β-protons is shifted downfield relative to the β-protons of **1a** (Supporting Information, Figure S1).

Crystal Structure. The crystal structure determination (Table 1) revealed that the asymmetric unit of **1a** contains one $[Ru(bpy)_2(3\text{-}TDP)]^+$ cation, one PF_6^- anion, and two

dx.doi.org/10.1021/ic2019204 | Inorg. Chem. 2012, 51, 1614−1624

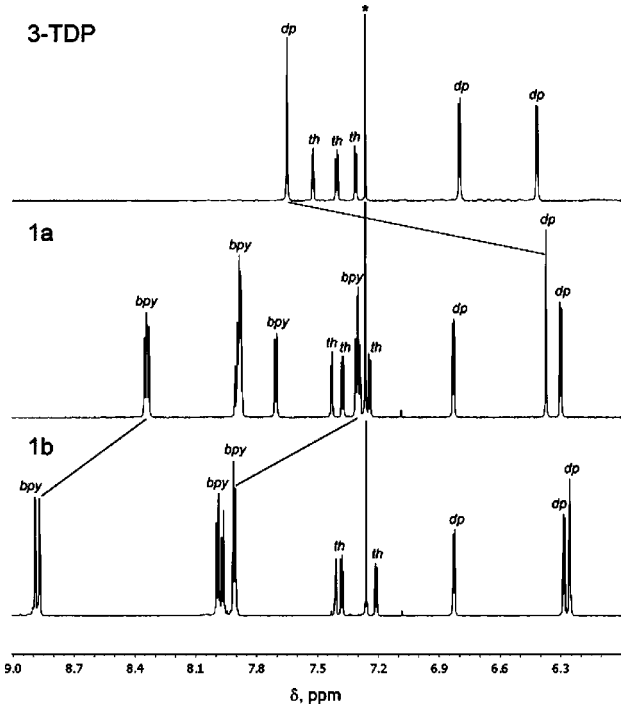

Figure 1. Aromatic region of ^{1}H NMR spectra of 3-TDP, **1a**, and **1b** ($CDCl_3$, room temperature). Proton signals that belong to bpy, thiophenyl, and dipyrrinato fragments are labeled as *bpy*, *th*, and *dp*, respectively. The residual solvent signal is marked with an asterisk. The solid black lines indicate the shift of α-protons of dipyrrin upon complexation to the Ru^{II} ion and the shifts of protons of bpy upon addition of carboxylate groups (see the text).

disordered chloroform molecules (Figure 2a). Pyrrole rings of the dipyrrinato ligand are essentially coplanar, while the thienyl ring is out of the dipyrrinato plane by 55° and exhibits two orientations rotated by 180° with respect to each other (in a 55% to 45% ratio). Complex **2** crystallizes as a neutral molecule (Figure 2b) without any interstitial solvent and exhibits a similar geometry and disorder of 3-TDP ligands, both of which are related by a 2-fold rotation axis. The dihedral angle between the dipyrrinato and the thienyl planes is 59°. The thienyl ring is disordered over two positions rotated by 180° with respect to each other and occurring in an 82% to 18% ratio.

Selected bond lengths and angles for complexes **1a** and **2** are listed in Table 2. Noteworthy, the Ru−N bond lengths, on average, are slightly longer for the 3-TDP ligands than for the bpy ligands, which can be explained by the decreased d-π back-bonding to the dipyrrinato ligand. The bite angle of bpy is close to 80°, while the bite angle of 3-TDP is close to 90° owing to the formation of the less strained six-membered chelating ring.

Electrochemistry. Electrochemical properties were evaluated by cyclic voltammetry (Table 3). All complexes exhibit a reversible oxidation process at positive potentials vs NHE, which corresponds to the Ru^{III}/Ru^{II} couple, as well as several quasi-reversible ligand reduction processes at negative potentials (Figure 3).

In comparison to $[Ru(bpy)_3](PF_6)_2$ ($E_{1/2}^{ox}$ = 1.52 V), the Ru^{III}/Ru^{II} redox couple in all the examined complexes is shifted to lower potentials, owing to the monoanionic nature of dipyrrinato ligands, which destabilize the t_{2g} orbitals of the Ru^{II} ion, making it easier to oxidize. The shift is more pronounced in the case of **2** ($E_{1/2}^{ox}$ = 0.31 V), which contains two $[3\text{-TDP}]^-$ ligands. Complex **1b** is oxidized at notably higher potential ($E_{1/2}^{ox}$ = 1.21 V) than **1a**, because of the strong electron-withdrawing effect of the ester substituents, which results in the stabilization of the reduced (Ru^{II}) state of the complex.

Similar considerations apply to the reduction potentials. Complexes with lower overall charge and ligands with better electron-donating ability result in higher electron density at Ru^{II}, increasing back-bonding and destabilizing the π^* orbitals of the ligands, thereby shifting their reduction potentials to more negative values. Similar changes in redox potentials have been reported for $[Ru(bpy)_2(ppy)]PF_6$, which also contains an anionic chelating ligand, ppy^- (Table 3).[12]

As follows from the preceding discussion, the oxidation is facilitated and the reduction is suppressed along the series **1b** → **1a** → **2**. Note, however, that in contrast to the other complexes, **1b** is not only more easily oxidized than $[Ru(bpy)_3]^{2+}$ but also reduced easier than this reference complex. This, of course, is a consequence of the electron-withdrawing effect of the ester groups. Nevertheless, it indicates that the HOMO−LUMO gap in **1b** is substantially lower than in $[Ru(bpy)_3]^{2+}$, owing to both the destabilization of the metal t_{2g} orbitals by the 3-TDP ligand and the stabilization of the bpy π^* orbitals by the ester substituents.

Electronic Spectroscopy. Electronic absorption spectra were recorded in acetonitrile solutions. All dipyrrinato-containing complexes exhibit three absorption bands in the

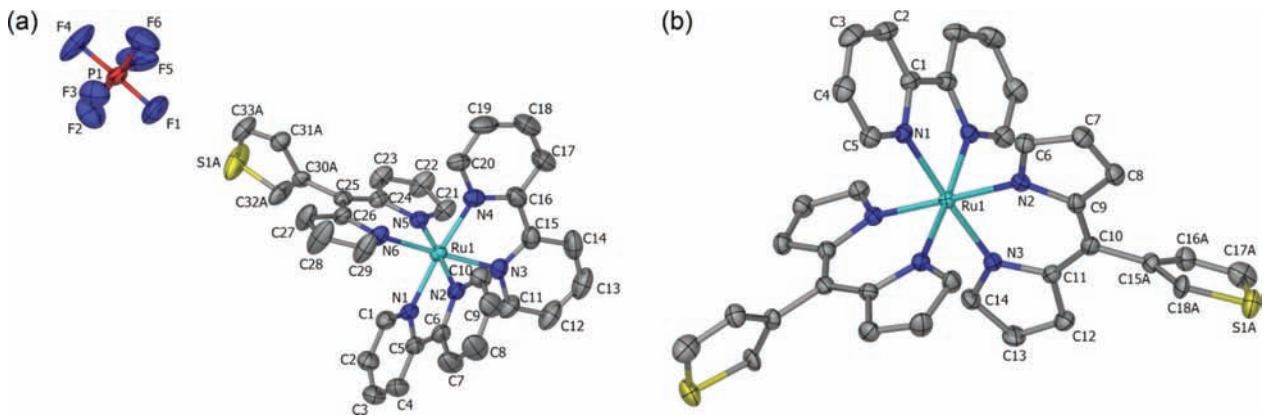

Figure 2. Crystal structures of **1a** (a) and **2** (b). Thermal ellipsoids at the 50% probability level. Hydrogen atoms and solvent molecules are omitted for the sake of clarity.

dx.doi.org/10.1021/ic2019204 | *Inorg. Chem.* 2012, 51, 1614−1624

Table 2. Selected Bond Lengths (Å) and Angles (deg) in the Crystal Structures of 1a and 2

[Ru(bpy)$_2$(3-TDP)](PF$_6$), **1a**				Ru(bpy)(3-TDP)$_2$, **2**			
Ru1−N1	2.041(4)	N1−Ru1−N2	79.5(1)	Ru1−N1	2.038(1)	N1−Ru1−N1′	79.37(8)
Ru1−N2	2.046(4)	N3−Ru1−N4	79.0(1)	Ru1−N2	2.069(1)	N2−Ru1−N3	88.58(6)
Ru1−N3	2.056(4)	N5−Ru1−N6	88.3(1)	Ru1−N3	2.061(1)		
Ru1−N4	2.061(3)						
Ru1−N5	2.067(3)						
Ru1−N6	2.068(4)						

Table 3. Electrochemical Properties of 1a, 1b, and 2[a]

complex	solvent	$E_{1/2}^{ox}$, V	$E_{1/2}^{red1}$, V	$E_{1/2}^{red2}$, V	$E_{1/2}^{red3}$, V
[Ru(bpy)$_3$](PF$_6$)$_2$[b]	MeCN	1.52	−1.10	−1.29	−1.54
[Ru(bpy)$_2$(ppy)]PF$_6$[13]	MeCN	0.70	−1.36	−1.62	
[Ru(bpy)$_2$(3-TDP)]PF$_6$ (**1a**)	MeCN	0.90	−1.16	−1.45	−1.77
[Ru(dcmb)$_2$(3-TDP)]PF$_6$ (**1b**)[c]	CH_2Cl_2	1.21	−0.78	−1.14	−1.47
Ru(bpy)(3-TDP)$_2$ (**2**)[d]	THF	0.31	−1.52	−1.73	

[a]All potentials have been referenced to the NHE. [b]Measured in this work as a reference complex. [c]The oxidized form is not soluble in MeCN. [d]The electrochemical window of MeCN is too narrow at negative potentials.

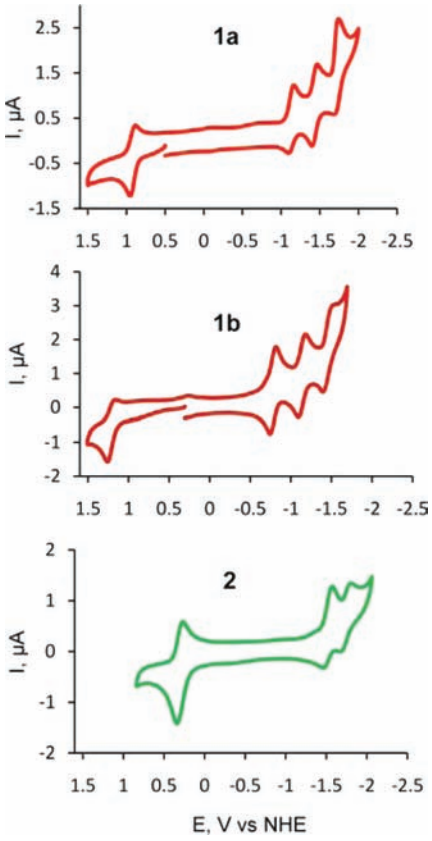

Figure 3. Cyclic voltammograms of **1a**, **1b**, and **2** recorded in 0.1 M solutions of (TBA)PF$_6$ in MeCN, CH_2Cl_2, and THF, respectively.

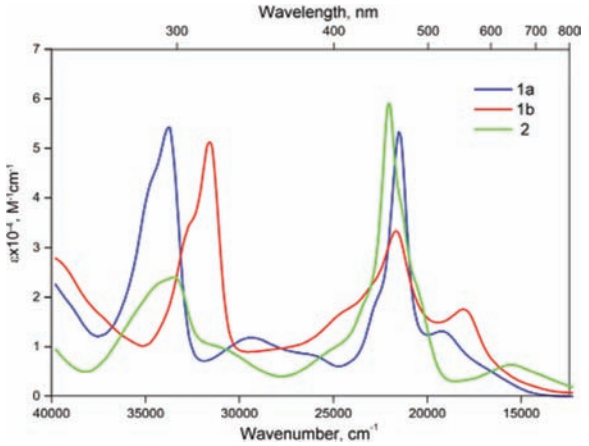

Figure 4. Electronic absorption spectra of **1a**, **1b**, and **2** recorded in acetonitrile solutions.

Table 4. Electronic Transitions in Complexes 1a, 1b, and 2[a]

	absorption maximum, nm ($\varepsilon \times 10^{-4}$, M^{-1} cm^{-1})		
complex	MLCT	dipyrrin $\pi-\pi^*$	bpy $\pi-\pi^*$
[Ru(bpy)$_3$](PF$_6$)$_2$[b]	451 (1.43)		280 (7.40)
[Ru(bpy)$_2$(3-TDP)](PF$_6$) (**1a**)	516 (1.30)	462 (5.34)	295 (5.45)
[Ru(dcmb)$_2$(3-TDP)](PF$_6$) (**1b**)	548 (1.74)	458 (3.33)	316 (5.16)
Ru(bpy)(3-TDP)$_2$ (**2**)	636 (0.62)	450 (5.92)	298 (2.40)
Ru(dcbpy)$_2$(NCS)$_2$ (N3)[4]	534 (1.42)		313 (3.12)

[a]Absorption spectra were recorded in MeCN solutions. [b]Measured in this work as a reference complex.

250−750 nm range (Figure 4). By comparison to the known spectra of the ligands and [Ru(bpy)$_3$]$^{2+}$ (Table 4),[45] the lower-energy band can be assigned to the MLCT transition, while the higher-energy band centered around 300 nm is due to the bpy $\pi-\pi^*$ transition. The strong intermediate-energy band that appears in the visible region corresponds to the characteristic optical absorption due to the dipyrrin $\pi-\pi^*$ transition. As expected, the intensities of the bpy $\pi-\pi^*$ transition and dipyrrin $\pi-\pi^*$ transition change in the opposite direction upon going from **1a** and **1b** to **2**, because of the change in the ratio of bpy to 3-TDP ligands.

For all the studied complexes, the MLCT band is red-shifted relative to the MLCT band of [Ru(bpy)$_3$]$^{2+}$. Similar to the trends observed in electrochemical properties, the red shift arises from the destabilization of the Ru t_{2g} orbitals by the monoanionic dipyrrinato ligand(s), which results in a smaller HOMO−LUMO gap and lowers the MLCT energy. The red shift is the largest for complex **2**, which contains two dipyrrinato ligands.

dx.doi.org/10.1021/ic2019204 | Inorg. Chem. 2012, 51, 1614−1624

Table 5. Energies[a] and Compositions[b] of Frontier MOs of Complexes 1a, 1b, and 2

	1a				1b[c]				2			
MOs	energy (eV)	Ru	3-TDP	bpy	energy (eV)	Ru	3-TDP	bpy	energy (eV)	Ru	3-TDP	bpy
LUMO+3	2.75	1.1	2.0	96.9	1.92	0.8	0.0	99.2	3.07	2.4	1.8	95.8
LUMO+2	2.03	5.9	0.2	93.9	1.87	1.2	91.2	7.7	2.26	3.3	96.4	0.4
LUMO+1	1.99	3.5	66.1	30.4	1.37	8.4	0.4	91.2	2.24	5.7	1.0	93.3
LUMO	1.98	0.7	30.4	68.9	1.31	4.1	0.6	95.3	2.16	0.4	97.4	2.2
HOMO	−1.13	72.6	19.1	8.3	−1.36	0.7	99.1	0.2	−0.51	72.1	25.0	3.0
HOMO−1	−1.19	68.1	22.7	9.2	−1.49	65.3	26.2	8.5	−0.64	76.2	19.4	4.4
HOMO−2	−1.25	0.7	98.9	0.4	−1.54	61.8	28.6	9.6	−0.74	70.3	19.3	10.4
HOMO−3	−1.43	78.4	5.1	16.5	−1.84	76.7	5.5	17.8	−1.00	0.1	99.8	0.1

[a]All energies have been converted to the NHE scale assuming that the NHE potential is −4.5 V vs vacuum level (see ref 47). [b]The percent contribution of the three constituent moieties (the Ru metal center and the 3-TDP and bpy ligands) to each MO is shown. [c]To make calculations less time-consuming, a hydrogen atom was substituted for each methyl group in **1b**. This change should not affect the results and conclusions to a significant extent.

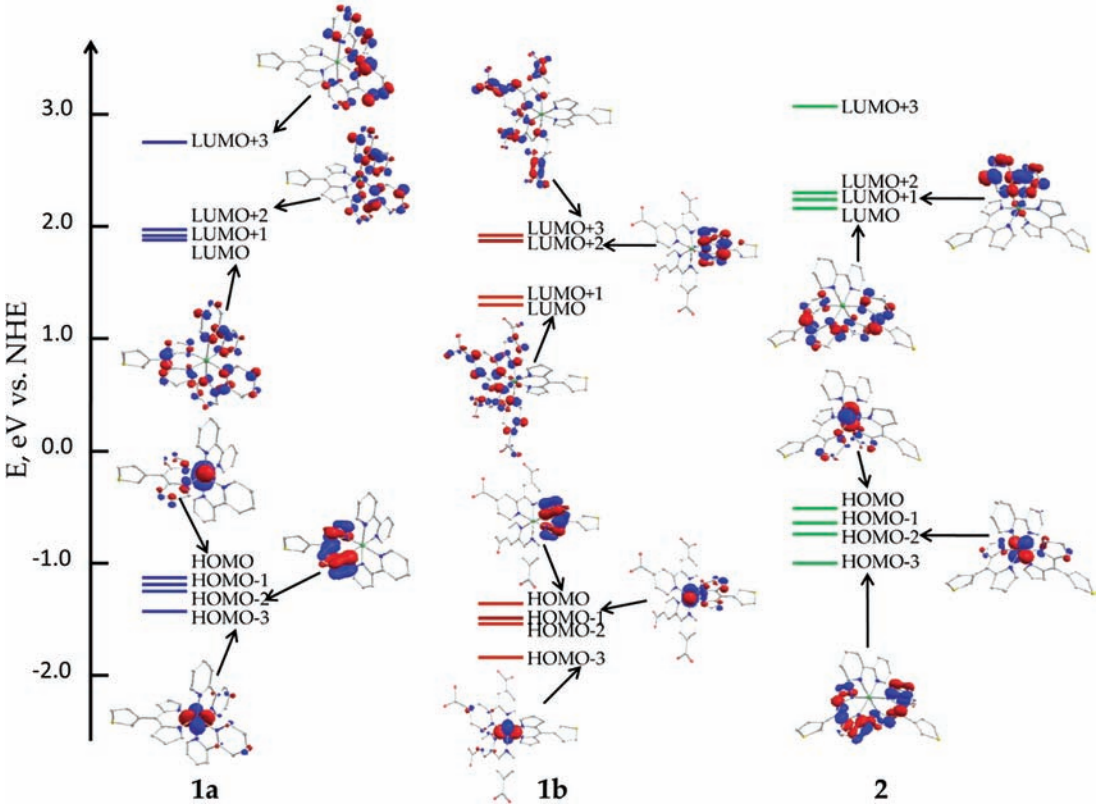

Figure 5. Frontier MOs of complexes **1a**, **1b**, and **2**. H atoms have been omitted for clarity. All energies have been converted to the NHE scale assuming that the NHE potential is −4.5 V vs vacuum level.[47]

The most remarkable observation comes from the comparison of spectra of **1a** and **1b**. The introduction of ester groups in the latter leads to the red shift and dramatic increase in intensity of the MLCT band (compare $\varepsilon = 1.30 \times 10^4$ M^{-1} cm^{-1} at 516 nm for **1a** and $\varepsilon = 1.74 \times 10^4$ M^{-1} cm^{-1} at 548 nm for **1b**). Furthermore, the dipyrrin $\pi-\pi^*$ transition becomes substantially broadened in **1b**. The red shift of the MLCT band is attributed to the electron-withdrawing nature of the ester groups, which stabilize bpy π^* orbitals giving rise to a lower HOMO−LUMO gap. The ester groups also extend the conjugated system of bpy, an effect that was shown to enhance the extinction coefficient of the corresponding MLCT transition.[6] With respect to the benchmark N3 dye, complex **1b** exhibits an additional intense band due to the dipyrrin $\pi-\pi^*$ transition (458 nm, $\varepsilon = 3.33 \times 10^4$ M^{-1} cm^{-1}), which further enhances its light-harvesting capacity. No emission was observed for either of complexes **1a**, **1b**, and **2**, which can be explained by the energy gap law: the decrease in the energy difference between the ground and the excited states results in the exponential increase of the rate constant for nonradiative decay.[46]

DFT Calculations and Electronic Structure. To elucidate the electronic structure and gain further insight into the electrochemical and optical properties of **1a**, **1b**, and **2**, DFT calculations were performed using the B3LYP hybrid functional and TZVP basis set (DZVP for Ru). The energies of the frontier MOs and contributions from the Ru center and 3-TDP and bpy ligands are listed in Table 5, while the energy diagram and selected MOs are depicted in Figure 5. The calculations on complex **1a** reveal that Ru d-orbitals make major contributions

dx.doi.org/10.1021/ic2019204 | Inorg. Chem. 2012, 51, 1614−1624

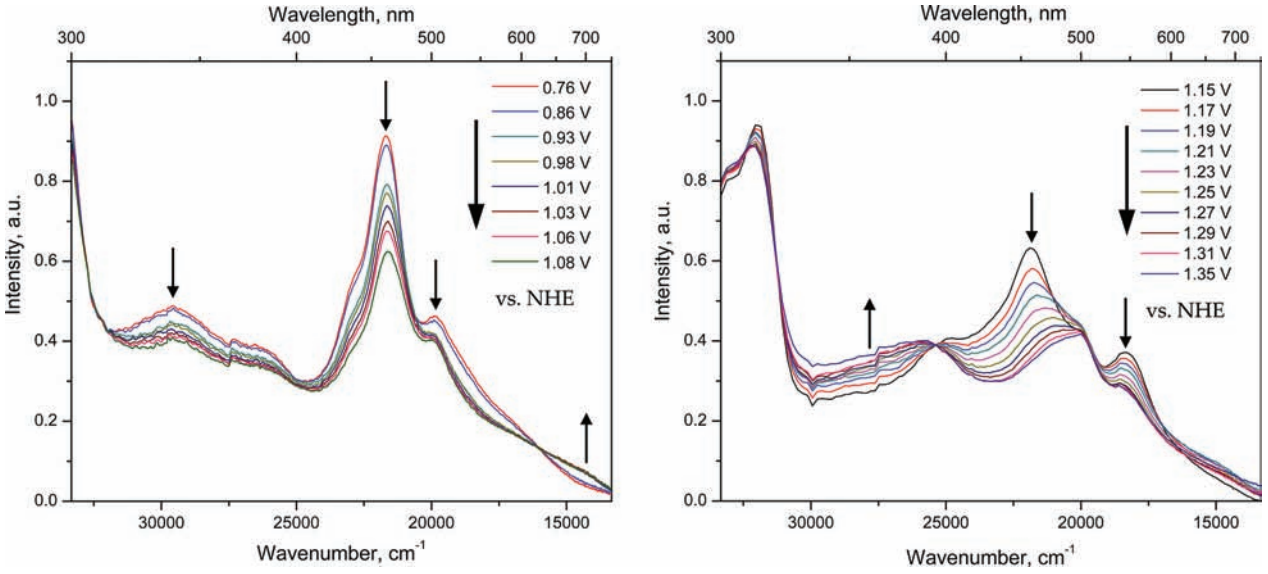

Figure 6. Thin-layer absorption spectra of **1a** (a) and **1b** (b) recorded in acetonitrile solution at different applied potentials (vs NHE). The spectral evolution resulting from sequential changes in the applied potential is indicated with black arrows.

to three occupied frontier orbitals, HOMO, HOMO−1, and HOMO−3 (72.6%, 68.1%, and 78.4%, respectively), although some electron density of these MOs is also found on the 3-TDP ligand (19.1%, 22.7%, 5.1%). Thus, these orbitals can be considered to have a metal−ligand character. Only ∼0.1 eV below the HOMO lies the HOMO−2 that is localized almost completely on 3-TDP (98.9%). The nearly degenerate LUMO and LUMO+1 are ligand-based, with comparable contributions from 3-TDP and bpy, while the LUMO+2 is 0.04 eV higher in energy and essentially bpy-based.

For comparison and as a reference point, we also calculated the energies of the HOMO and the LUMO of $[Ru(bpy)_3]^{2+}$ at the same level of theory. These were found to be −1.82 and 1.72 V vs NHE, respectively. It can be clearly seen that both occupied and unoccupied frontier orbitals of **1a** are raised in energy relative to the $[Ru(bpy)_3]^{2+}$ values, which is also in accord with the results of electrochemical studies, as **1a** has a less positive oxidation potential and a more negative reduction potential as compared to $[Ru(bpy)_3](PF_6)_2$ (Table 3). Calculations on 1e-oxidized and 1e-reduced forms of **1a** revealed that the majority of spin density in the oxidized **1a** is localized on the Ru center (Supporting Information, Figure S4a), thus confirming that the oxidation process for **1a** is metal-based. The first reduction of **1a** occurs on the 3-TDP ligand (Supporting Information, Figure S4b), which allows assignment of the second and third negative-potential processes observed for **1a** to consecutive reductions of bpy ligands.

To study the effect of electron-withdrawing substituents in complex **1b**, the calculations were performed on its carboxylic acid analogue (all methyl groups in **1b** were replaced with H atoms). The introduction of carboxylic groups stabilizes the Ru d-orbitals and leads to a change in the order of energies of the frontier occupied orbitals (Figure 5, Table 5). The HOMO of **1b** is localized on 3-TDP, while the HOMO−1 and HOMO−2 are lower in energy (by 0.13 and 0.18 eV, respectively) and delocalized over the metal and 3-TDP. Similarly, owing to the presence of electron-withdrawing groups, the LUMO and LUMO+1 are localized on bpy and appear substantially lower in energy (by 0.56 and 0.50 eV, respectively) than the next unoccupied orbital, the 3-TDP-based LUMO+2.

Overall, the frontier orbitals of **1b** are shifted to lower energies relative to those of **1a** (Table 5 and Figure 5). This trend is in good agreement with the electrochemical data. The introduction of electron-withdrawing substituents in **1b** stabilizes the frontier orbitals and shifts the oxidation and reduction potentials to more positive values (Table 3). Interestingly, it also affects the character of the oxidized and reduced species. The calculations of the spin density distribution in the 1e-oxidized and 1e-reduced forms of **1b** show that the oxidation takes place on 3-TDP and not on the Ru center (Supporting Information, Figure S5a), while the first reduction occurs on the bpy moiety (Supporting Information, Figure S5b). This points yet again to the strong stabilization of the π^* orbitals of bpy relative to the π^* orbital of 3-TDP because of the presence of the electron-withdrawing carboxylic groups in **1b**.

To verify these results experimentally, we carried out thin-layer spectroelectrochemical measurements on **1a** and **1b** by scanning the potential of the first redox wave in fixed steps and recording the absorption spectrum after reaching equilibrium at the corresponding voltage. In agreement with the theoretical calculations, the complexes exhibit substantially different behavior. Upon oxidation, the changes in the position of the MLCT and 3-TDP $\pi-\pi^*$ bands in the spectrum of **1a** are rather small (Figure 6a). The maximum of the former is shifted from 504 to 497 nm, while the position of the latter remains essentially unchanged, although its intensity in the spectrum of $\mathbf{1a}^+$ is significantly decreased. In contrast, the 3-TDP $\pi-\pi^*$ transition of **1b** is strongly affected by the oxidation, with its maximum being shifted from 458 to 498 nm, while the shift in the MLCT band is less evident (Figure 6b). These results support the theoretical finding that the first oxidation in **1b** takes place at the 3-TDP ligand.

Simulated absorption spectra (Figure 7) obtained by TD-DFT calculations using the optimized geometries of **1a** and **1b** reproduce well the experimentally observed spectra, although the simulated spectra have a slight blue shift relative to the experimental ones. (Detailed band assignments are provided in the Supporting Information, Table S1). The lowest-energy band of **1a**, with the experimental maximum at 19,380 cm^{-1} (516 nm), corresponds to HOMO−1→LUMO+1 and HOMO−3→LUMO

dx.doi.org/10.1021/ic2019204 | Inorg. Chem. 2012, 51, 1614−1624

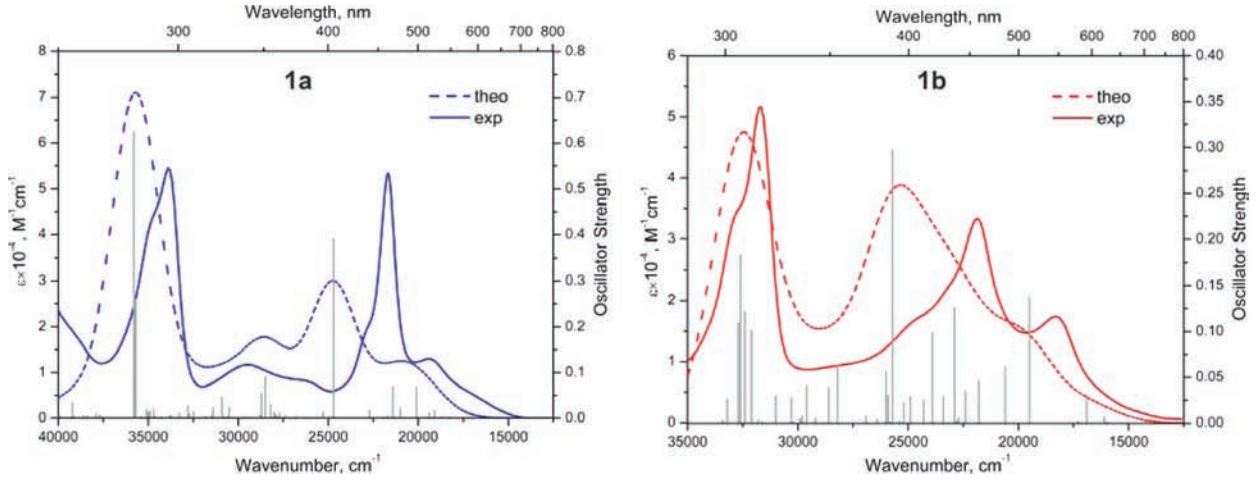

Figure 7. Experimental (solid line) and simulated (dashed line) absorption spectra of **1a** and **1b**. The gray bars indicate the energy and oscillator strength of each electronic excitation.

electronic excitations, both of which are primarily of MLCT character and involve electron transfer from the Ru t_{2g} orbitals to π^* orbitals of both 3-TDP and bpy ligands. The strong absorption at 21,650 cm^{-1} (462 nm) is assigned to excitations from HOMO−2 to LUMO+1 and LUMO, which correspond to intraligand $\pi-\pi^*$ (3-TDP) and interligand $\pi-\pi^*$ (3-TDP→bpy) transitions, respectively. The weaker band with the maximum at 26,670 cm^{-1} (375 nm) is due to HOMO−1→LUMO+5 and HOMO→LUMO+6 transitions, which are mainly of MLCT (Ru t_{2g} → bpy π^*) type.

As the order of orbital energies in **1b** is affected by the electron-withdrawing substituents, so is the character of the electronic absorption bands. An examination of TD-DFT results indicates that the lowest-energy band with the experimental maximum at 18,250 cm^{-1} (548 nm) corresponds to HOMO−2→LUMO+1 and HOMO−3→LUMO+1/LUMO electronic excitations, which are described as Ru t_{2g} → bpy π^* MLCT processes, not involving π^* orbitals of 3-TDP, in contrast to the lowest-energy MLCT band of **1a**. The next band in the simulated electronic absorption spectrum of **1b** appears significantly broadened as compared to the corresponding band of **1a** (Figure 7), which again agrees with experimental findings. The maximum of the band corresponds to $\pi-\pi^*$ type HOMO→LUMO+2/LUMO+5 excitations from the π orbital of 3-TDP to the π^* orbital of 3-TDP or bpy, respectively. The shoulders of the band are mainly of MLCT character. The red-side shoulder is due to transitions from HOMO−1, HOMO−2, and HOMO−3 to LUMO+3 and LUMO+5 and the blue-side shoulder is composed of HOMO−2→LUMO+6 and HOMO−3→LUMO+4 transitions, all of which correspond to excitations from Ru t_{2g} orbitals to bpy π^* orbitals. Similar contributions to the red and blue sides of the $\pi-\pi^*$ band are observed in **1a**, but in the case of **1b** they exhibit stronger overlaps with the $\pi-\pi^*$ band, which make the latter appear much broader.

The introduction of the second 3-TDP ligand in complex **2** results in destabilization of Ru d orbitals, which is clearly reflected in the results of DFT calculations. The three highest occupied MOs are mainly centered on Ru, with a smaller contribution coming from 3-TDP. The highest π orbital of 3-TDP, HOMO−3, appears 0.26 eV below the Ru-based HOMO−2. The lowest four unoccupied MOs alternate between 3-TDP (LUMO and LUMO+2) and bpy (LUMO+1 and LUMO+3). These orbitals are destabilized to much lesser extent than the

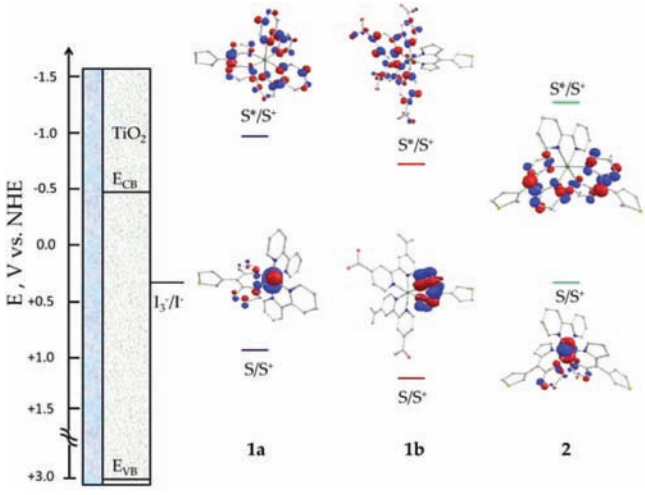

Figure 8. Energy states of **1a**, **1b**, and **2** with respect to the bottom of conduction band (E_{CB}) of TiO_2 and the I_3^-/I^- redox couple (the energies of S/S^+ and S^*/S^+ were calculated using $E_{1/2}^{ox}$ and the low-energy threshold of corresponding absorption spectrum, respectively).

Ru-based orbitals (Table 5), which is in agreement with the observed electrochemical behavior (Table 3). The calculations on the 1e-oxidized and 1e-reduced forms of **2** support the aforementioned assignment of the first oxidation process to the oxidation of the Ru center (Supporting Information, Figure S6a) and indicate that the first reduction takes place on the 3-TDP ligands (Supporting Information, Figure S6b). According to TD-DFT calculations (Supporting Information, Figure S7), and similar to **1a** and **1b**, the lowest-energy band is mainly due to MLCT-type HOMO−2→LUMO/LUMO+1 and HOMO−1→LUMO+2 excitations. The next band is composed predominantly of HOMO−3/HOMO−4→LUMO/LUMO+2 excitations, which correspond to $\pi-\pi^*$ transitions of 3-TDP.

CONCLUDING REMARKS

As demonstrated above, the Ru complexes of 3-TDP act as strong panchromatic light absorbers in the visible region. Nevertheless, to be viable candidates for light-harvesting applications, in particular for DSSCs, the orbital energies of these complexes should be appropriately positioned with respect to the conduction band of TiO_2 and the redox potential of the

dx.doi.org/10.1021/ic2019204 | Inorg. Chem. 2012, 51, 1614−1624

I_3^-/I^- hole-transporting couple. Upon inspection of the Ru^{III}/Ru^{II} redox processes observed for complexes **1a** and **2**, it becomes immediately obvious that the latter is not an appropriate candidate for this purpose, as its oxidation potential nearly coincides with the potential of the I_3^-/I^- couple (Figure 8). The oxidation potential of **1a**, however, does appear below the I_3^-/I^- potential, which incited us to explore its carboxylated version, **1b**, for future attachment to the surface of TiO_2 nanoparticles. In this complex, the oxidation potential is lowered even more relative to that of **1a**, while the overlap of various absorption bands is increased. In addition, the π^* orbitals of bpy are stabilized with respect to the π^* orbital of 3-TDP. Consequently, the observed MLCT transitions have almost exclusively Ru $t_{2g} \rightarrow$ bpy π^* character and do not involve the π^* orbital of 3-TDP. Moreover, as demonstrated by the DFT calculations and spectroelectrochemical measurements, the hole in the oxidized complex $\mathbf{1b}^+$ is localized on the 3-TDP ligand. These features are desirable for improving charge injection into the conduction band of TiO_2 via the dcbpy ligand (4,4′-dicarboxylato-2,2′-bipyridine) attached to the surface of the semiconductor and preventing charge recombination by localizing the hole further from the semiconductor surface. The investigation of the performance of complex **1b** as a sensitizer in a DSSC device is currently in progress and will be reported in due course.

■ ASSOCIATED CONTENT

Supporting Information

Crystallographic information files, additional 1-D and 2-D ^1H NMR spectra, mass-spectra, plots of spin-density distribution in the oxidized and reduced forms of the complexes, a simulated absorption spectrum of **2**, theoretical assignment of electronic transitions in **1a**, **1b**, and **2**. This material is available free of charge via the Internet at http://pubs.acs.org.

■ AUTHOR INFORMATION

Corresponding Author

*E-mail: shatruk@chem.fsu.edu (M.S.), gorelsky@gmail.com (S.I.G.).

Present Address

⊥Department of Chemistry, University of California at Davis, Davis, CA 95616, U.S.A.

■ ACKNOWLEDGMENTS

M.S. gratefully acknowledges the Florida State University for the support of this work through the CRC Planning Grant. S.I.G. thanks the Centre for Catalysis Research and Innovation (CCRI) for funding and computing resources.

■ REFERENCES

(1) Vlachopoulos, N.; Liska, P.; Augustynski, J.; Grätzel, M. *J. Am. Chem. Soc.* **1988**, *110*, 1216−1220.

(2) Grätzel, M. *Inorg. Chem.* **2005**, *44*, 6841−6851.

(3) Nazeeruddin, M. K.; De Angelis, F.; Fantacci, S.; Selloni, A.; Viscardi, G.; Liska, P.; Ito, S.; Takeru, B.; Grätzel, M. *J. Am. Chem. Soc.* **2005**, *127*, 16835−16847.

(4) Nazeeruddin, M. K.; Kay, A.; Rodicio, I.; Humphry-Baker, R.; Müller, E.; Liska, P.; Vlachopoulos, N.; Grätzel, M. *J. Am. Chem. Soc.* **1993**, *115*, 6382−6390.

(5) Ardo, S.; Meyer, G. J. *Chem. Soc. Rev.* **2009**, *38*, 115−164.

(6) Nazeeruddin, M. K.; Péchy, P.; Renouard, T.; Zakeeruddin, S. M.; Humphry-Baker, R.; Comte, P.; Liska, P.; Cevey, L.; Costa, E.; Shklover, V.; Spiccia, L.; Deacon, G. B.; Bignozzi, C. A.; Grätzel, M. *J. Am. Chem. Soc.* **2001**, *123*, 1613−1624.

(7) Wang, P.; Zakeeruddin, S. M.; Moser, J. E.; Nazeeruddin, M. K.; Sekiguchi, T.; Grätzel, M. *Nat. Mater.* **2003**, *2*, 402−407.

(8) Wang, P.; Klein, C.; Humphry-Baker, R.; Zakeeruddin, S. M.; Grätzel, M. *J. Am. Chem. Soc.* **2005**, *127*, 808−809.

(9) Chang, W. C.; Chen, H. S.; Li, T. Y.; Hsu, N. M.; Tingare, Y. S.; Li, C. Y.; Liu, Y. C.; Su, C.; Li, W. R. *Angew. Chem., Int. Ed.* **2010**, *49*, 8161−8164 , S8161-1.

(10) Bessho, T.; Yoneda, E.; Yum, J. H.; Guglielmi, M.; Tavernelli, I.; Imai, H.; Rothlisberger, U.; Nazeeruddin, M. K.; Grätzel, M. *J. Am. Chem. Soc.* **2009**, *131*, 5930−5934.

(11) Wu, K. L.; Hsu, H. C.; Chen, K.; Chi, Y.; Chung, M. W.; Liu, W. H.; Chou, P. T. *Chem. Commun.* **2010**, *46*, 5124−5126.

(12) (a) Bomben, P. G.; Robson, K. C. D.; Sedach, P. A.; Berlinguette, C. P. *Inorg. Chem.* **2009**, *48*, 9631−9643. (b) Bomben, P. G.; Koivisto, B. D.; Berlinguette, C. P. *Inorg. Chem.* **2010**, *49*, 4960−4971.

(13) Robson, K. C. D.; Koivisto, B. D.; Yella, A.; Sporinova, B.; Nazeeruddin, M. K.; Baumgartner, T.; Grätzel, M.; Berlinguette, C. P. *Inorg. Chem.* **2011**, *50*, 5494−5508.

(14) Chen, C. Y.; Wu, S. J.; Wu, C. G.; Chen, J. G.; Ho, K. C. *Angew. Chem., Int. Ed.* **2006**, *45*, 5822−5825.

(15) Chen, C. Y.; Chen, J. G.; Wu, S. J.; Li, J. Y.; Wu, C. G.; Ho, K. C. *Angew. Chem., Int. Ed.* **2008**, *47*, 7342−7345.

(16) Gao, F.; Wang, Y.; Zhang, J.; Shi, D.; Wang, M.; Humphry-Baker, R.; Wang, P.; Zakeeruddin, S. M.; Grätzel, M. *Chem. Commun.* **2008**, 2635−2637.

(17) Chen, C. Y.; Wang, M.; Li, J. Y.; Pootrakulchote, N.; Alibabaei, L.; Ngoc-Le, C. H.; Decoppet, J. D.; Tsai, J. H.; Grätzel, C.; Wu, C. G.; Zakeeruddin, S. M.; Grätzel, M. *ACS Nano* **2009**, *3*, 3103−3109.

(18) Haugland, R. P. *Handbook of fluorescent probes and research chemicals*, 9th ed.; Molecular Probes Inc.: Eugene, OR, 2011.

(19) Li, F.; Yang, S. I.; Ciringh, Y.; Seth, J.; Martin, C. H.; Singh, D. L.; Kim, D.; Birge, R. R.; Bocian, D. F.; Holten, D.; Lindsey, J. S. *J. Am. Chem. Soc.* **1998**, *120*, 10001−10017.

(20) Erten-Ela, S.; Yilmaz, M. D.; Icli, B.; Dede, Y.; Icli, S.; Akkaya, E. U. *Org. Lett.* **2008**, *10*, 3299−3302.

(21) Kolemen, S.; Cakmak, Y.; Erten-Ela, S.; Altay, Y.; Brendel, J.; Thelakkat, M.; Akkaya, E. U. *Org. Lett.* **2010**, *12*, 3812−3815.

(22) Wood, T. E.; Thompson, A. *Chem. Rev.* **2007**, *107*, 1831−1861.

(23) Smalley, S. J.; Waterland, M. R.; Telfer, S. G. *Inorg. Chem.* **2009**, *48*, 13−15.

(24) Yadav, M.; Singh, A. K.; Maiti, B.; Pandey, D. S. *Inorg. Chem.* **2009**, *48*, 7593−7603.

(25) (a) McLean, T. M.; Cleland, D. M.; Lind, S. J.; Gordon, K. C.; Telfer, S. G.; Waterland, M. R. *Chem.—Asian J.* **2010**, *5*, 2036−2046. (b) Hall, J. D.; McLean, T. M.; Smalley, S. J.; Waterland, M. R.; Telfer, S. G. *Dalton Trans.* **2010**, *39*, 437−445.

(26) Robertson, N. *Angew. Chem., Int. Ed.* **2006**, *45*, 2338−2345.

(27) Fulmer, G. R.; Miller, A. J. M.; Sherden, N. H.; Gottlieb, H. E.; Nudelman, A.; Stoltz, B. M.; Bercaw, J. E.; Goldberg, K. I. *Organometallics* **2010**, *29*, 2176−2179.

(28) Pavlishchuk, V. V.; Addison, A. W. *Inorg. Chim. Acta* **2000**, *298*, 97−102.

(29) Maiti, N.; Lee, J.; Do, Y.; Shin, H. S.; Churchill, D. G. *J. Chem. Crystallogr.* **2005**, *35*, 949−955.

(30) Wiederholt, K.; McLaughlin, L. W. *Nucleic Acids Res.* **1999**, *27*, 2487−2493.

(31) Bennett, M. A.; Huang, T. N.; Matheson, T. W.; Smith, A. K. *Inorg. Synth* **1982**, *21*, 74−78.

(32) Evans, I. P.; Spencer, A.; Wilkinson, G. *J. Chem. Soc., Dalton Trans.* **1973**, 204−209.

(33) *SMART and SAINT*; Bruker AXS Inc.: Madison, WI, 2007.

(34) Sheldrick, G. M. *SADABS*; University of Göttingen: Göttingen, Germany, 1996.

(35) Sheldrick, G. M. *Acta Crystallogr., Sect. A* **2008**, *A64*, 112−122.

(36) Frisch, M. J.; Trucks, G. W.; Schlegel, H. B.; Scuseria, G. E.; Robb, M. A.; Cheeseman, J. R.; Scalmani, G.; Barone, V.; Mennucci,

B.; Petersson, G. A.; Nakatsuji, H.; Caricato, M.; Li, X.; Hratchian, H. P.; Izmaylov, A. F.; Bloino, J.; Zheng, G.; Sonnenberg, J. L.; Hada, M.; Ehara, M.; Toyota, K.; Fukuda, R.; Hasegawa, J.; Ishida, M.; Nakajima, T.; Honda, Y.; Kitao, O.; Nakai, H.; Vreven, T.; Montgomery, Jr., J. A.; Peralta, J. E.; Ogliaro, F.; Bearpark, M.; Heyd, J. J.; Brothers, E.; Kudin, K. N.; Staroverov, V. N.; Kobayashi, R.; Normand, J.; Raghavachari, K.; Rendell, A.; Burant, J. C.; Iyengar, S. S.; Tomasi, J.; Cossi, M.; Rega, N.; Millam, N. J.; Klene, M.; Knox, J. E.; Cross, J. B.; Bakken, V.; Adamo, C.; Jaramillo, J.; Gomperts, R.; Stratmann, R. E.; Yazyev, O.; Austin, A. J.; Cammi, R.; Pomelli, C.; Ochterski, J. W.; Martin, R. L.; Morokuma, K.; Zakrzewski, V. G.; Voth, G. A.; Salvador, P.; Dannenberg, J. J.; Dapprich, S.; Daniels, A. D.; Farkas, Ö.; Foresman, J. B.; Ortiz, J. V.; Cioslowski, J.; Fox, D. J. *Gaussian 09*, Revision A.02; Gaussian Inc.: Wallingford, CT, 2009.

(37) Lee, C.; Yang, W.; Parr, R. G. *Phys. Rev. B* **1988**, *37*, 785−789.

(38) Becke, A. D. *J. Chem. Phys.* **1993**, *98*, 5648−5652.

(39) Godbout, N.; Salahub, D. R.; Andzelm, J.; Wimmer, E. *Can. J. Chem.* **1992**, *70*, 560−571.

(40) Schäfer, A.; Huber, C.; Ahlrichs, R. *J. Chem. Phys.* **1994**, *100*, 5829−5835.

(41) Gorelsky, S. I. *SWizard program*; University of Ottawa: Ottawa, Canada, 2010; http://www.sg-chem.net/.

(42) Gorelsky, S. I.; Lever, A. B. P. *J. Organomet. Chem.* **2001**, *635*, 187−196.

(43) Gorelsky, S. I. *AOMix: Program for molecular orbital analysis*, version 6.5; University of Ottawa: Ottawa, Canada, 2011; http://www.sg-chem.net/.

(44) Choi, S. H.; Kim, K.; Lee, J.; Do, Y.; Churchill, D. G. *J. Chem. Crystallogr.* **2007**, *37*, 315−331.

(45) Chiorboli, C.; Indelli, M. T.; Scandola, F. *Top. Curr. Chem.* **2005**, *257*, 63−102.

(46) Freed, K. F.; Jortner, J. *J. Chem. Phys.* **1970**, *52*, 6272−6291.

(47) Grätzel, M. *Nature* **2001**, *414*, 338−344.